On the pressure-induced loss of crystallinity in orthophosphates of zinc and calcium

Dmitry Shakhvorostov[a)] and Martin H. Müser
Department of Applied Mathematics, University of Western Ontario, London, Ontario N6A 5B7, Canada

Nicholas J. Mosey
Department of Mechanical and Aerospace Engineering, Princeton University, Princeton, New Jersey 08544-5263, USA

David J. Munoz–Paniagua
National Institute for Nanotechnology, Edmonton, Alberta T6G 2M9, Canada

Gavin Pereira, Yang Song, Masoud Kasrai, and Peter R. Norton
Department of Chemistry, University of Western Ontario, London, Ontario N6A 5B7, Canada

A recently suggested mechanism for the stress memory of various metal phosphates is investigated experimentally. Based on first-principles simulations [N. J. Mosey *et al.*, Science **307**, 1612 (2005)], it had been argued that atoms with flexible coordination, such as zinc or heavy-metal cations, act as network-forming agents, undergoing irreversible pressure-induced changes in bonding that lead to increased connectivity between phosphate anions. In the present study, orthophosphates of zinc and calcium were exposed to high pressures on surfaces and in diamond anvil cells. An additional set of first-principles simulations was accomplished on α-orthophosphate of zinc, which suggested that this material was already cross-linked before compression but that it nevertheless underwent a reversible coordination change under pressure in agreement with the experimental results presented here. Raman spectra indicate an irreversible, pressure-induced loss of long-range crystallinity. The pressures required to induce these changes are around 7 GPa for the zinc phosphates, while they are close to 21 GPa for the calcium phosphates. Hydrogenation of the metal phosphate lowers the threshold pressure by approximately 2–3 GPa in both cases. Moreover, α-orthophosphate of zinc could be partially amorphisized under nonisotropic pressure on copper foils. © *2008 American Institute of Physics*. [DOI: 10.1063/1.2837809]

I. INTRODUCTION

The mechanical properties of metal phosphates, in particular, their stress-history dependence, are of interest in areas of science and engineering ranging from planetary science to tribology. Indications for stress-history dependence were identified, for instance, in various heavy-metal phosphates stemming from meteoroids, which exhibited spectra of metastable phases.[1,2] Lead phosphate is a well-studied and paramount ferroelastic and, thus, also stress-history dependent.[3,4] Moreover, zinc phosphates (ZPs) are used in dental restoration as an important component of cements.[5] Perhaps the technologically most relevant application of metal phosphates is in their use as antiwear additives for steel engines.[6] Experiments on zinc-phosphate films, which had formed on steel surfaces under rubbing, indicate that the so-called antiwear films are stiffer on top of asperities, where pressure is highest, than at their edges.[7] Unfortunately, zinc phosphates do not appear to protect fuel-efficient, lightweight aluminum engines as well as they protect steel engines. For this reason and due to increasingly strict environmental constraints on lubricant additives, there is an urgent need to understand how zinc-phosphate films form and function, so that replacements can be designed in a more rational fashion than currently possible and less by trial and error.

A microscopic mechanism for the stress-history dependence of metal phosphates was suggested previously on the basis of first-principles molecular dynamics simulations in which systems composed of loosely connected ZP molecules were subjected to time-dependent external pressures.[8] The results demonstrated that zinc, which was tetrahedral in the initial structure at ambient pressures (although it fluctuated between di-, tri- and tetracoordinate states in some simulations) adopted a "seesaw" geometry when compressed to 6 GPa. (A tetracoordinate seesaw geometry can be derived by removing any two adjacent bond sites from a central atom with an originally hexacoordinate octahedral geometry.) The new coordination sites available at the zinc atom in this configuration led to the formation of bonds between zinc and oxygen atoms in neighboring phosphate chains. Although the net valency of zinc did not change in the process, the formation of the new bonds increased the degree of connectivity between the phosphate chains in the system, with zinc acting as the network-forming agent. Upon decompression to ambient pressures, the zinc atom reverted to a tetrahedral state; however, the Zn—O bonds associated with the increased connectivity in the system persisted. (When reaching pressures above 16 GPa, additional coordination changes oc-

a)Electronic mail: dshakhvo@uwo.ca.

curred, which did not affect the chemical bonds after decompression.) It was argued that this irreversible transformation of loosely connected ZPs into a highly connected ZP network and the concomitant effects on the mechanical properties of the system play an important role in the formation and functionality of ZP antiwear films.[9] Upon recompression, similar coordination changes occurred, although these turned out to be reversible.

The pressure-induced film formation and coordination change scenario are provocative because the macroscopic hardness of most engineering surfaces is smaller than the pressure required for the relevant chemical transformation to take place. The hypothesis, thus, asks for experimental verification. Two attempts so far have been negative. In one study, zinc dialkyldithiophosphate (ZDDP) molecules were exposed to high pressures[10] and no irreversible changes in the local structure could be detected at room temperature, either with Raman or with infrared spectroscopy. All changes were characterized as loss of crystallinity. However, this finding does not disprove the theory. ZDDP decomposes under engine conditions and, thus, the "inactive" ZDDP was studied in Ref. 10 rather than a functional decomposition product. Zinc phosphates might only become active after some running in time.[11] A second study on α-Zn$_3$(PO$_4$)$_2$, which can be seen as a model substance for the decomposition product of ZDDP, did not show irreversible changes either.[12] The spectroscopy used, however, was only sensitive to the vibrations of the tetrahedral PO$_4$ units. While we do not (mean to) disagree with the findings of that study, analysis of the molecular structures produced in the simulation reveals that the P—O radial distribution function remains unaltered after decompression and that all computable changes occur on the Zn—O radial distribution function. Thus, more work is required to assess the validity of the calculations themselves; i.e., the predicted chemical changes under pressure, and to determine the relevance of the anticipated reaction to the antiwear effectiveness of ZPs.

In the present study, we will focus on three questions. First, do ZPs undergo the predicted processes when subjected to the idealized condition of isotropic stress that was imposed in the simulations? Second, can similar reactions be induced on surfaces, where stresses are applied anisotropically and may be limited by factors such as the macroscopic hardness of the surface material? Third, how sensitive are the observed processes to the chemical nature of the system? The answers to these questions are pertinent to assessing the validity of the theory derived from the simulations and to the broader field of lubricant engineering. However, the discussion of the results within the context of lubricant engineering will necessarily be speculative in nature, pending further studies to investigate the relationship between the processes discussed here and those occurring under tribological conditions.

In order to investigate the hypothesis that the pressure irreversibly modifies the bonding at zinc, we have performed experiments in which ZPs were exposed to isotropic and anisotropic pressures. Several spectroscopic techniques were used to probe the structural details of the systems at various stages of (de)compression and to look for evidence of irre-

versible transformations. To closely reproduce the calculations, we sought to study systems that were similar in chemical structure and composition to those explored in the simulations. The systems used in the simulations had chemical compositions ranging from ZnP$_5$O$_{18}$H$_9$ to Zn$_2$P$_7$O$_{26}$H$_{13}$ and were composed of loosely connected molecules of Zn(PO$_4$H$_2$)$_2$ and P$_3$O$_{10}$H$_5$.[8] Unfortunately, it was not possible to synthesize such systems. Instead the experiments were performed using α-Zn$_3$(PO$_4$)$_2$. This material is readily available and has been investigated recently by Gauvin *et al.*[12] as a model for ZDDP antiwear films. Although the chemical composition of this system differs from the models explored in the simulations, the local bonding at zinc under ambient conditions is similar in both cases; i.e., zinc is bonded to four oxygen atoms. Furthermore, the structure of crystalline α-Zn$_3$(PO$_4$)$_2$ is well-known, which will aid in interpreting the results. Experiments using Ca$_3$(PO$_4$)$_2$ were also performed to investigate the effect of replacing zinc, while hydrogenated zinc and calcium phosphates were used to study the influence of hydrogen on any observed processes.

The remainder of this article will be organized as follows. In Sec. II, we describe experimental and computational methods. Numerical results in addition to those presented in Ref. 8 are presented in Sec. III. Section IV contains the results from Raman experiments on various phosphates from nonhydrogenated zinc phosphates to hydrogenated calcium phosphates. Experimental data on the structure (x ray) and the chemistry [x-ray photoelectron spectroscopy (XPS) and x-ray absorption near edge structure (XANES)] are provided in Secs. V and VI, respectively. Conclusions are drawn in Sec. VII.

II. METHODS

A. Simulation details

First-principles molecular dynamics (MD) simulations of α-Zn$_3$(PO$_4$)$_2$ were performed to complement the experiments. The simulations were performed on a single unit cell of α-Zn$_3$(PO$_4$)$_2$, and periodic boundary conditions were employed to treat this system as a bulk material. The α-ZPs were compressed/decompressed by applying isotropic, time-dependent pressures and allowing the size and shape of the simulation cell to vary in response to the changes in pressure.[13] This procedure ultimately applies the pressure to the atoms in the system, thereby permitting pressure-induced chemical reactions.

The specific details associated with the (de)compression of the system are as follows. First, the system was equilibrated at a temperature of 300 K and at ambient pressure. The external pressure was then increased linearly at a rate of 10.0 GPa/ps until a maximum pressure $P_{max}=15$ GPa was reached. The pressure was then decreased at the same rate until a final pressure of 1 bar was attained. Overall, this procedure mimics the changes in pressure experienced in the experiments, where the ZPs are compressed/decompressed over a range of pressures spanning several gigapascals. However, it is important to note that the rate of (de)compression employed in the simulations is significantly higher than that

used in the experiments, which will likely preclude thermal activation in the simulations. Hence, the pressures required to induce processes in the simulations upon compression will be higher and upon decompression will be lower than those required to induce similar processes in the experiments.

The simulations were performed within the Car-Parrinello MD extended Lagrangian formalism[14] with the CPMD software package,[15] which we modified to allow the applied pressure to vary with time. The electronic structure was solved using Kohn-Sham density functional theory[16] with the exchange-correlation functional of Perdew, Burke, and Ernzerhof.[17] The valence electrons were represented by a set of plane waves expanded at the Γ point up to a kinetic energy cutoff of 120 Ry, and the core elecrons were represented with norm-conserving pseudopotentials.[18] Tests on ZPs indicate that this simulation methodology yields pressures that agree to within 0.2 GPa of those obtained with a plane wave cutoff of 200 Ry. The nuclear coordinates were propagated using a time step of 2.0 a.u. and the fictitious electron mass was set at 400 a.u. This conserved the total energy of the system to better than 10^{-5} a.u./ps.

B. Experimental details

In this study, samples are exposed to isotropic and nonisotropic stresses. Characterization of the chemical and crystalline structure was done by Raman, x-ray diffraction (XRD), XPS, and XANES. The advantage of Raman is that it can be used *in situ* during compression. Unfortunately, it cannot directly probe the bonding on zinc because the vibrations of zinc are not directly involved in Raman active vibrational modes. Most of the peaks in the spectra of zinc orthophosphate arise due to stretching and bending modes of PO_4 groups.[19,20] Nevertheless, the symmetric stretching mode of PO_4 group had been found previously to be sensitive to the zinc bond arrangements[19] in phosphates with different zinc coordinations. Moreover, Raman reacts sensitively to long-range order; i.e., clear peaks can be identified in crystalline polyphosphate powders, while amorphous polyphosphate shows broadened peaks. Information about chemical connectivity of zinc, oxygen, and phosphor was obtained by XPS and XANES on samples before compression and after decompression.

1. Raman spectroscopy and diamond anvil cell technique

For isotropic compression, a symmetric piston-cylinder type of diamond anvil cell (DAC) equipped with 400 μm culet diamond anvils was used. A few ruby (Cr^{+3} doped α-Al_2O_3) chips as pressure calibrant were carefully placed inside the gasket sample chamber before the sample was loaded. The pressure was determined from the well-known pressure shift of the R_1 ruby fluorescence line (at 694.2 nm under ambient conditions) with an accuracy of ± 0.05 GPa under quasihydrostatic conditions.[21]

A commercial Renishaw Raman spectrometer (model 2000) was used for pressure determination and Raman measurements. This model is a compact laser Raman microprobe capable of both spectroscopy and imaging. A HeNe laser (632.8 nm) was used as the excitation source with average power of several milliwatts on the sample. An edge filter is installed to remove the Rayleigh and anti-Stokes lines enabling a measurable spectral range of above 120 cm^{-1}. The spectrometer is further equipped with an imaging spectrograph and a sensitive thermoelectronically cooled charged coupled device (CCD) detector allowing a spectral resolution of 1 cm^{-1}. Spectral calibration of the Raman spectrum was realized using silicon and diamond standards achieving an accuracy of ± 0.5 cm^{-1}. The spectra were collected in the range of 120–1300 cm^{-1}. This spectral range covered all the Raman active modes of PO_4.

Purity of all phosphates obtained from Aldrich is 99.999% except $Zn(H_2PO_4)_2$, which was prepared as described in Ref. 22. The structure of the latter was verified using x-ray diffraction. The samples were loaded at room temperature as powder with nominal pressure slightly above ambient. Then, the cell is carefully pressurized with small steps and allowed to stabilize for a few minutes after each pressure change before Raman spectra were taken. Experiments were conducted up to 20 GPa and reproduced for a few times.

Nonisotropic pressures were investigated as well. This was done with a flat punch to better mimic tribological situations. Nonisotropic stresses were obtained by pressing two self-adjusting half spheres against each other. The specimens were placed on a copper foil to reduce pressure irregularities.

2. XPS

The XPS analyses were carried out with a Kratos Axis Ultra spectrometer using monochromatized Al $K\alpha$ x rays. The high resolution spectra (± 0.2 eV) were obtained (160 eV pass energy) in hybrid mode and the analyzed area was 50 μm in diameter. The spectra were processed using CASAXPS software and quantified using sensitivity factors supplied by Kratos.

3. XANES

XANES data on phosphorus were obtained at the Canadian Synchrotron Radiation Facility (CSRF). Phosphorus K-edge spectra were collected on the double-crystal monochromator[23] covering an energy range of 1500–4000 eV with photon resolution of 0.8 eV. The zinc L edge was obtained at the Canadian Light Source using spherical grating monochromator capable of covering an energy range of 250–2000 eV with a photon resolution of greater than 5000. Phosphorus L-edge spectra were obtained on the Grasshopper soft x-ray beamline covering an energy range of 70–900 eV with a photon resolution of 0.2 eV. The phosphorus K and L edges and the zinc L edge were calibrated using pure unreacted di-isobutyl ZDDP. The analyzed area was about 1 mm^2. The photoabsorption spectra for both the model compounds and samples were recorded in the total electron yield mode and fluorescence yield mode for both surface and bulk sensitivities.[24] All spectra shown in this paper are an average of two scans that were digitally combined and normalized, with a linear background subtracted.
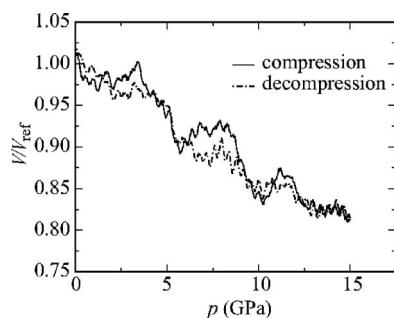
FIG. 1. Equation of state for a compression/decompression cycle of α-Zn$_3$(PO$_4$)$_2$ as obtained from first-principles calculations.

The assignment of the fine structure in XANES was carried out using model compounds obtained by the authors or by comparison to previous results.[11,25,26]

4. XRD

XRD was used to validate our assumptions on the initial structure of the zinc phosphate used in experiments. Additionally, decompressed samples were analyzed to ascertain if pressure-induced structural changes had taken place.

The XRD data were collected on a SMART6000 CCD camera with a three-circle D8 diffractometer, parallel focused cross-coupled mirrors, on a Rigaku RU200 rotating anode Cu x-ray generator. The power was set to 50 kV/90 mA and a 0.20 mm beam collimator was used. The goniometer was positioned with all angles at zero, and exposure time was 240 s in transmission. Corundum was used to calibrate detector center and distance (5.17 cm). Data collection software was Bruker SMART. Data analyses were Bruker GADDS, Bruker TOPAS, and POWDERCELL for ASCII conversion.

III. COMPUTATIONAL RESULTS

The MD simulations provide detailed atomic-level insight regarding the effect of pressure on the structure of the system. This information allows one to identify the bonds that are affected by compression, which will aid in the interpretation of the experimental results. In what follows, the results of the MD simulations of α-Zn$_3$(PO$_4$)$_2$ will be examined along with a reinvestigation of our previous MD simulations of ZnP$_5$O$_{18}$H$_9$,[8] which were used to develop the cross-linking theory.

The calculated equation of state for α-Zn$_3$(PO$_4$)$_2$ is shown in Fig. 1. During compression, the system underwent rapid drops in volume at pressures of approximately 4 and 9 GPa. The hysteresis-free volume change at 4 GPa appears to be physical in nature without chemical change in the tetracoordinate state of zinc. Meanwhile, the drop at 9 GPa coincided with the formation of an additional Zn—O bond at some of the zinc atoms, causing these atoms to become pentacoordinate. The zinc atoms remained in the pentacoordinate state as the system was compressed to a maximum pressure of 15 GPa. During decompression, the zinc atoms reverted to a tetracoordinate state at a pressure of approximately 5 GPa. Note that this is lower than the pressure of 9 GPa that was necessary to induce the transition to the pen-

tacoordinate state during compression. This difference in the transition pressures is the origin of the hysteresis that exists between 5 and 9 GPa. Upon complete decompression, the bonding in the system was consistent with that in crystalline α-Zn$_3$(PO$_4$)$_2$ and, thus, the pressure-induced transitions observed during the simulations were completely reversible.

These results can be compared with our previous simulations of ZnP$_5$O$_{18}$H$_9$.[8] In those simulations, the bonding at the zinc atom became unstable when the pressure reached 6 GPa. This led to irreversible changes in bonding that increased the connectivity between the phosphate chains in the system. Due to the increased connectivity, the decompressed system occupied significantly less volume than it did prior to compression. The difference in the volume of the system before and after compression was said to have been caused by a "run-in loop." In the simulations of α-Zn$_3$(PO$_4$)$_2$, pressure-induced instabilities were also observed; although, the resultant changes in the bonding at zinc were reversible upon complete decompression. Since the system reverted to the initial structure upon complete decompression, no "run-in" effects were observed. It should also be noted that no P—O bonds were formed or broken at any point during the simulations of either ZP system.

It may be worthwhile to also compare the present simulation results to those obtained for zinc-free triphosphates, P$_3$O$_{10}$H$_5$.[27] In the latter system, a low-pressure hysteresis upon compression and decompression was found to be "viscous" in nature, similar to the low-pressure hysteresis found here. A second high-pressure hysteresis, which occurred at around 26 GPa, could be linked to a chemical reaction, in which some phosphorus atoms became pentavalent.

The behavior of the ZPs can be rationalized in terms of their structures prior to compression. In the case of ZnP$_5$O$_{18}$H$_9$, the initial structure was composed of loosely connected ZP molecules. These molecules included chains comprising several phosphate units and contained oxygen atoms that were involved in P=O and O—H bonds. These oxygen atoms can readily participate in the formation of Zn—O bonds, leading to new connections between the phosphate chains. Additionally, the flexibility of these chains allows them to adapt to the structural changes associated with increased connectivity. In the case of α-Zn$_3$(PO$_4$)$_2$, the initial system was a crystalline structure in which the zinc atoms were connected through individual PO$_4^{3-}$ units. These phosphate units exhibited the maximum possible level of connectivity prior to compression, with each oxygen atom involved in at least one Zn—O bond. As such, the degree of connectivity between the phosphate units in this system cannot be increased. Despite this, it is possible to alter the specific Zn—O bonds that are present in the system, which is a critical feature of the cross-linking theory. For instance, when zinc is in the pentacoordinate state adopted above 9 GPa, there exist five Zn—O bonds—four that were present in the original crystalline structure and one "new" Zn—O bond. The simulations showed that the zinc reverts to a tetracoordinate state upon decompression, which requires the dissociation of one of these bonds. In the simulations of α-ZP described above, the new Zn—O bond dissociated in all cases, which amounts to the zinc atom returning
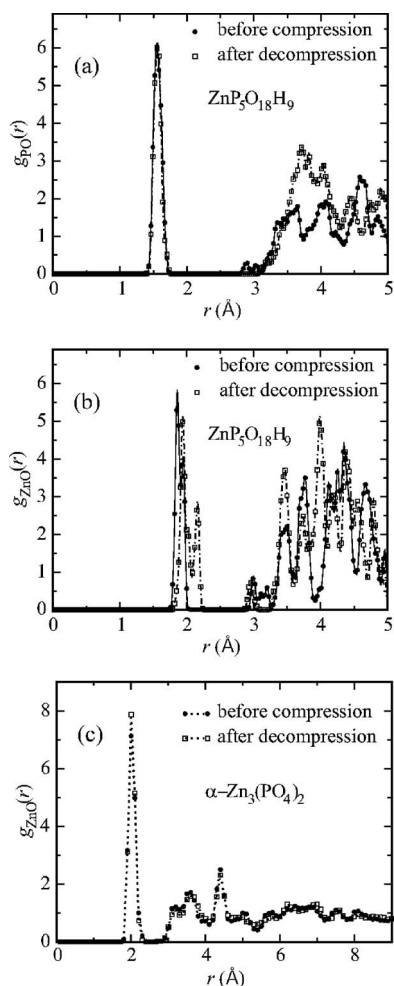
FIG. 2. Radial distribution functions obtained from first-principles calculations. (a) $g_{PO}(r)$ for $ZnP_5O_{18}H_9$, (b) $g_{ZnO}(r)$ for $ZnP_5O_{18}H_9$, and (c) $g_{ZnO}(r)$ for α-$Zn_3(PO_4)_2$.

to its original position in the crystalline structure. In order for the new Zn—O bond to persist when the zinc returns to a tetracoordinate state upon decompression, the zinc atom must move to a location that differs from its position in the original crystal. Such motion of zinc atoms was inhibited in the simulations due to artificial topological constraints that result from the use of a small simulation cell and periodic boundary conditions. However, the mobility of the zinc atoms would increase in the absence of these constraints, e.g., in experiments, resulting in either amorphization or the adoption of short-range crystallinity.

To more quantitatively investigate the effect of pressure on the bonding within the ZPs, we have calculated the Zn—O and P—O radial distribution functions for $ZnP_5O_{18}H_9$ and α-$Zn_3(PO_4)_2$ before compression and after decompression. These are given in Fig. 2. The data pertaining to the P—O bonding in $ZnP_5O_{18}H_9$ indicate that the PO_4 unit is unaffected by pressure. The data obtained from the simulation of α-$Zn_3(PO_4)_2$, which are not shown, led to the same conclusion. In contrast, the Zn—O bonds in the two ZPs respond differently to compression. In the case of $ZnP_5O_{18}H_9$, compression clearly leads to an irreversible change in the bonding at Zn. Meanwhile the Zn—O bonds

in α-$Zn_3(PO_4)_2$ are unaffected by pressure. These observations are consistent with the qualitative discussion of the simulations provided above.

The different behaviors of $ZnP_5O_{18}H_9$ and α-$Zn_3(PO_4)_2$ can be understood as follows: In α-$Zn_3(PO_4)_2$, any atom can be reached from any other atom by passing exclusively through covalent or mixed covalent-ionic bonds. One may, thus, argue that the system is already cross-linked prior to the first compression. This differs from the situation for the model decomposition products for ZDDP: The molecules were considered to be chemically passivated with hydrogens so that reaching an atom in another molecule required passing through a van der Waals bond. Some hydrogen termination popped off in the initial compression, thereby allowing the network formation process. Despite this discrepancy between the compounds, both systems have the common feature that the coordination changes on zinc upon a second compression at relatively low pressures.

Overall, the MD simulations indicate that any significant pressure-induced (irreversible) changes within the ZPs should involve Zn—O bonds, while the bonding at phosphorus will remain largely unaltered. The Raman spectroscopy used to study the structure of the ZPs (see below) is sensitive to P—O bonds, while the Zn—O bonds are Raman inactive. Thus, Raman cannot be used to directly probe the bonding at zinc, yet can be used to test the prediction that the P—O bonds are unaffected by compression. The lack of changes in the P—O bonding would be evident from the absence of significant shifts in the Raman peaks. Raman spectroscopy is also sensitive to the loss of long-range crystallinity, which manifests itself as a broadening of the peaks. As a result, this method can be used to detect irreversible changes in the structure of the system involving either amorphization or the formation of short-range crystallinity. As noted above, such transformations can result from changes in the Zn—O bonds of α-$Zn_3(PO_4)_2$; although, it is also possible for the irreversible loss of crystallinity to arise through entirely different processes. In order to determine whether any observed loss of crystallinity is actually the result of changes in the Zn—O bonds, it will be necessary to employ other spectroscopic methods that are sensitive to these bonds.

IV. RAMAN RESULTS

A. Nonhydrogenated zinc phosphates

DAC experiments were performed in which α-$Zn_3(PO_4)_2$ was compressed from ambient pressure to different maximum pressures P_{max} and then decompressed. Raman spectra were obtained at various stages of the experiments to look for evidence of changes in the P—O bonds and the long-range crystalline order of the material. The Raman spectrum of the original uncompressed sample is given at the top in Fig. 3 and exhibits characteristic features that will be monitored as the system is compressed. These features include triplet structures at around 1000 and 550 cm^{-1} and peaks within the 100–300 cm^{-1} range of frequencies. The triplet structure at 1000 cm^{-1} is associated with the P—O bonds, with the peak at 960 cm^{-1} corresponding to the symmetric stretching of the PO_4 unit and the other two peaks

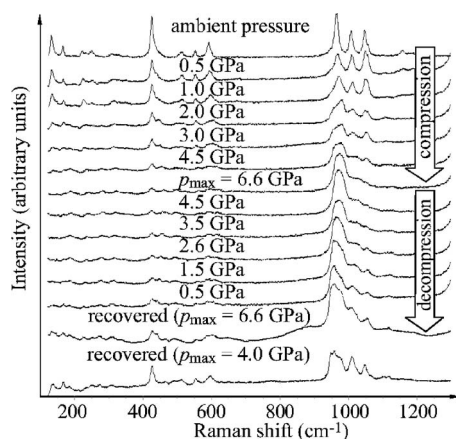FIG. 3. Raman spectra of α-Zn$_3$(PO$_4$)$_2$ measured during a compression-decompression cycle. Pressure inside the sample chamber is indicated over each spectra. The comparison of recovered structures from 4.0 and 6.6 GPa is given at the bottom of the figure.

FIG. 4. Raman spectra of α-Zn$_3$(PO$_4$)$_2$ as powder, polycrystalline bulk, and amorphous bulk. The width of the peaks is related to the long-range order. Raman spectra of polyphosphate glasses with PO$_3$ groups, whose P—O vibrations occur at higher wave numbers as compared to those of PO$_4$ groups (Refs. 29–31).

relating to antisymmetric vibrational modes. The peaks at lower frequencies are related to the long-range order of the system.

A series of Raman spectra taken at various stages of (de)compression are provided in Fig. 3. These spectra demonstrate that the triplet structure at 1000 cm^{-1} is affected by increasing the pressure. Specifically, the peak at 960 cm^{-1} is split and broadened, while the intensities of the other two peaks are significantly decreased. Compression also induces the loss of peaks in the low-frequency range of the spectrum. The bottom two spectra, which were obtained from decompressed samples, show that both the triplet structure and the low-frequency peaks are largely recovered if the system is exposed to a maximum pressure of 4 GPa, although the intensities of the peaks are altered. On the other hand, the spectrum obtained after decompressing the sample from 6.6 GPa shows that the triplet-peak structure and low-frequency peaks have been lost.

Overall, the DAC experiments indicate that subjecting the ZPs to P_{max}=6.6 GPa is sufficient to induce irreversible changes in the structure of the system. The broadening of the peak at 960 cm^{-1} combined with the loss of peaks in the low-frequency region are indicative of a loss of long-range order. This conclusion is supported by x-ray spectroscopy studies of ZPs exposed to a range of pressures, which suggest that the irreversible changes in the Raman spectra are accompanied by either amorphization or the adoption of a fine-crystalline structure (see Sec. V). It is also important to note that the symmetric stretching peak at 960 cm^{-1} is not shifted irreversibly by compression, which suggests that the phosphate units have remained intact. Had the bonding at phosphorus changed considerably, one would anticipate large shifts in the peaks associated with the P—O bonds as indicated by the representative Raman spectra of several different ZPs provided in Fig. 4.

The results of the DAC experiments are similar to those reported recently by Gauvin *et al.*,[12] who demonstrated that compressing ZPs to pressure of 20 GPa induced amorphization while leaving the phosphate unit intact. However, those authors did not explore intermediate pressure ranges. Here,
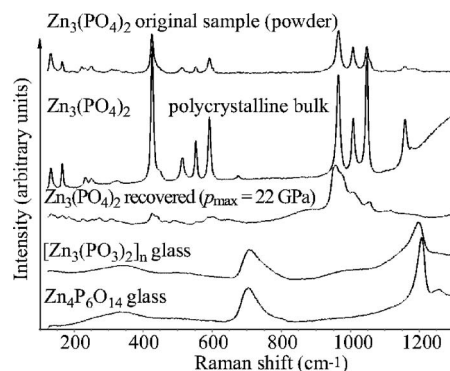
we have more precisely determined the amorphization pressure as 6.6 GPa. Furthermore, the results are consistent with the MD simulations, which indicated that the phosphate unit should remain intact.

α-ZPs were exposed to two additional pressure protocols. DAC experiments were performed with P_{max}=20 GPa to investigate the possibility that additional (irreversible) changes in structure occur at higher pressures. Moreover, the influence of anisotropic compression was considered in "punch" experiments where an estimated maximum pressure of 10 GPa was attained. The results of both sets of experiments are summarized in Fig. 5.

The results of the DAC experiments with P_{max}=20 GPa are similar to those with P_{max}=7 GPa. During compression, the triplet structure disappears and the symmetric stretching peak originally at 960 cm^{-1} shifts to higher frequencies. The intensities of the lower frequency peaks are decreased significantly as the pressure is increased. The spectrum obtained upon complete decompression from 20 GPa is nearly identical to that obtained with P_{max}=7 GPa, indicating that the higher pressures do not induce any additional changes in the structure of the system.

Analysis of the copper foil bearing the ZPs in the punch experiments showed regions of varying brightness that could be identified as copper, ZPs exposed to low pressures, and
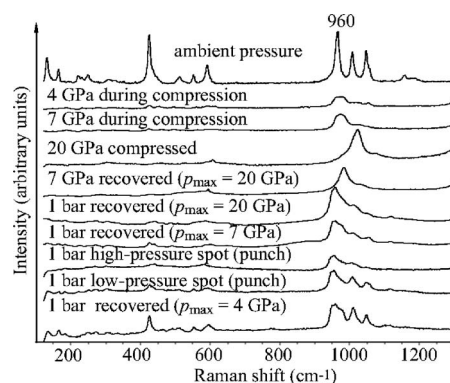

FIG. 5. Summary of Raman spectra of zinc phosphates compressed isotropically in a diamond anvil cell (DAC) and in a punch experiment (external pressure is applied uniaxially).

ZPs exposed to high pressures. These high- and low-pressure zones were associated with hills and valleys, which one can distinguish depending on lighting. Moreover, zones that are plastically deformed surface differ from that of polished and ground surface.

It is possible to focus on specific low-or high-pressure areas with Raman spectroscopy. Results are provided in Fig. 5. The spectrum taken from the high-pressure region is similar to that obtained in the DAC experiments with P_{max} =7 GPa. This is a key result because it indicates that the transformations observed in the DAC experiments can occur on surfaces in spite of the fact that the macroscopic hardnesses of the surface materials (Cu foil: 1.4 GPa and austenitic steel: 5 GPa) are lower than the pressures required to induce those changes. It is also important to note that the spectrum taken from the low-pressure region is consistent with that obtained in the DAC experiments with P_{max} =4 GPa, which indicates that the changes in the structure of the system are indeed pressure induced. Thus, the pressure-mediated transformations can be induced on top of surfaces that deform plastically underneath and may occur under tribological conditions.

B. Hydrogenated zinc phosphates

So far, our experiments have focused on systems composed of only Zn, O, and P. However, antiwear films derived under tribological conditions from ZDDP additives will most likely contain other elements, which will affect the details of the pressure-induced transitions. Hydrogen is one element that is almost certainly present in these antiwear films in the form of O—H bonds. Since hydrogen is highly mobile, it will become squeezed out of its bonding environment as the pressure is increased. This will lead to large local stresses, which may induce transitions at lower macroscopic pressures than those observed in the DAC simulations of nonhydrogenated ZPs. Furthermore, the dissociation of the O—H bonds will free up oxygen atoms to participate in the formation of new Zn—O bonds, while preventing the hydrogen atoms from returning to their original position in the material. This will also facilitate changes in Zn—O bonding leading to amorphization at lower pressures.

To investigate the effect of hydrogen on the pressure-induced behavior of ZPs, DAC experiments were performed on $Zn(H_2PO_4)_2$ using the procedure described above. A series of Raman spectra obtained at various stages of compression is provided in Fig. 6. The peaks associated with the O—H bonds are not shown due to high fluorescence in that specific range of frequencies; however, a doublet structure associated with the P—O bonds is evident at approximately 1000 cm^{-1}. As the system is compressed to P_{max}=5 GPa, this structure is broadened and shifted to higher frequencies. Upon complete decompression, these peaks have been altered irreversibly in a manner that is consistent with amorphization.

Additionally, the loss of the peaks near 200 cm^{-1} in the P_{max}=5 GPa experiment is indicative of the loss of long-range crystallinity. These results indicate that the presence of hydrogen decreases the amorphization pressure by approxi-
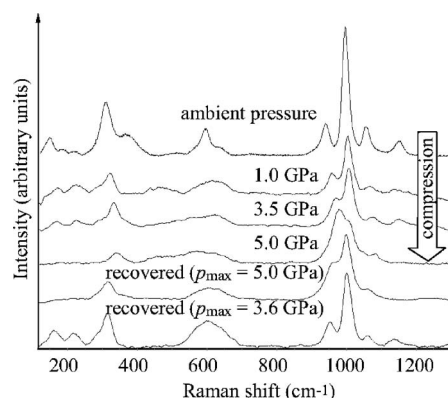

FIG. 6. Raman spectra of $Zn(H_2PO_4)_2$ during compression-decompression cycle. Pressure inside the sample chamber is indicated over each spectra. The comparison of recovered structures from 3.6 and 5.0 GPa is given at the bottom of the figure.

mately 2 GPa. As argued in more detail at the end of Sec. IV, this reduction can be rationalized in terms of hydrogen playing the role of a network modifier.

It is worth noting that the MD simulations indicated that hydrogenated ZPs undergo pressure-induced changes in structure at lower pressures (6 GPa) than nonhydrogenated ZPs (9 GPa). In the case of the hydrogenated ZPs, the transitions were accompanied by the motion of hydrogen atoms. However, in the absence of a better understanding of the atomic-level changes occurring in the experiments, it is not possible to definitely conclude that the effects of hydrogen observed in the experiments and simulations arise from the same origin.

C. Calcium phosphates

Calcium has been investigated as a potential replacement for zinc in antiwear additives. Moreover, calcium is present in significant amounts in lubricant detergents such as calcium sulfonate and becomes incorporated into the antiwear films. The effects of incorporating calcium into the films have been investigated, with the results indicating that the presence of this element decreases the ability of the film to protect steel surfaces from wear.[31–35]

In light of these experimental observations, we sought to determine whether the high-pressure behavior of calcium phosphates differs from that reported above for zinc phosphates. To achieve this, DAC experiments were performed in which $Ca_3(PO_4)_2$ was exposed to high pressures. The results are provided in Fig. 7 and indicate that pressure of 21 GPa must be achieved to induce irreversible changes in the structure of the calcium phosphates. In Sec. VI, we show that XANES and XPS spectra of the samples do not indicate any chemical changes and, thus, the Raman spectra are once again indicative of amorphization.

The amorphization pressure for calcium phosphates (21 GPa) is significantly higher than that of the zinc phosphates (7 GPa), indicating that the high-pressure behavior of metal phosphates is sensitive to the nature of the cation. Further studies will be necessary to ascertain whether the large
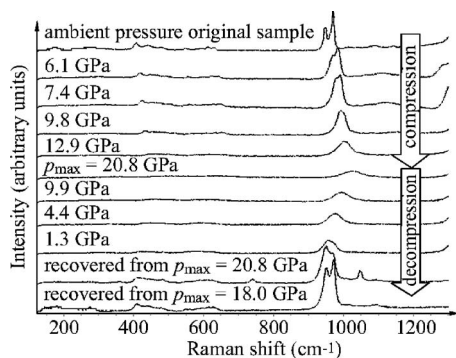
FIG. 7. Raman spectra of $Ca_3(PO_4)_2$ during compression-decompression cycle. Pressure inside the sample chamber is indicated over each spectrum. The comparison of recovered structures from 18.0 and 20.8 GPa is given at the bottom of the figure.

FIG. 9. (Color online) X-ray diffraction pattern measured on pristine powder and samples that were decompressed from different maximum pressures. The pattern calculated from the configuration used in the the first-principles calculation is shown as well.

difference in the amorphization pressure is related to significant differences in the antiwear capabilities of zinc and calcium phosphates.

DAC experiments were also performed on hydrogenated calcium phosphates. The results are summarized in Fig. 8 and demonstrate a decrease in the amorphization pressure to 16.5 GPa. This is analogous to the results obtained for the ZPs, where it was found that hydrogenation decreased the amorphization pressure by approximately 2 GPa. Once again, the decrease in pressure likely arises from the mobility of the hydrogen atoms, which leads to large local stresses, "frees up" oxygen atoms to form new Ca—O bonds, and prevents the system from returning to its original crystalline structure.

V. XRD

To obtain more precise structural information on the ZPs, samples from the DAC experiments were investigated with XRD. The results, which are presented in Fig. 9 and discussed in the next paragraph, are consistent with the conclusions drawn based on the evidence provided by Raman experiments.

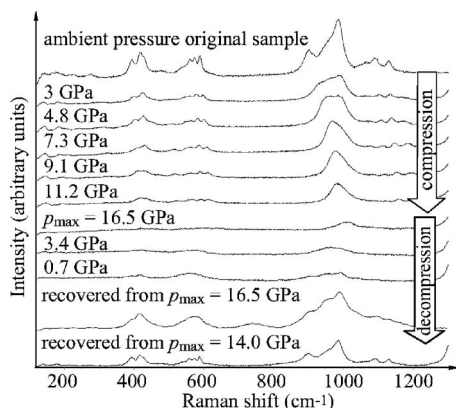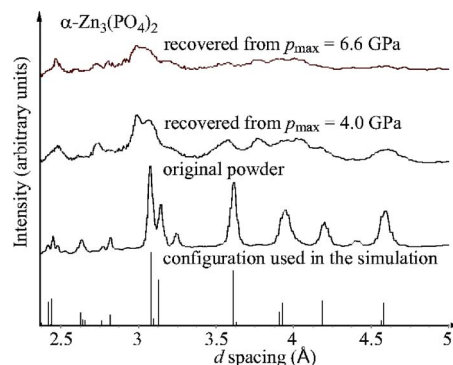We wish to note that the spectrum, which was computed from the α-zinc phosphate structure used in the first-

principles calculations is essentially identical to that of the original sample. Peaks were already broader for those samples that had been exposed to $P_{max} = 4.0$ GPa. However, the features from the uncompressed sample are still clearly evident. The sample that had been compressed to $P_{max} = 6.6$ GPa mainly shows diffuse scattering; although, it is evident that spacings of <3.5 Å are still clearly distinguishable. Most specific features are lost in the long-range region. In particular, the line associated with a 4.5 Å spacing disappears if $P_{max} = 6.6$ GPa, while it still occurs for the $P_{max} = 4.0$ GPa specimen.

VI. XANES AND XPS

Measurements of the binding energies of electrons (BEs) on zinc, phosphorus, and oxygen confirm the expectations from the simulations on $\alpha-Zn_3(PO_4)_2$. No significant change of the BE of the inner $2p$ orbital of zinc could be observed (see Fig. 10). The phosphate binding energies were consistent with the values found for other tetrahedral PO_4 units. It may be noted that the carbon $1s$ reference peak was set at 284.8 eV.

Figure 11 shows the XANES data for the zinc L edge for $\alpha-Zn_3(PO_4)_2$ after compression to various pressures, fol-

FIG. 8. Raman spectra of $CaHPO_4$ during compression-decompression cycle. Pressure inside the sample chamber is indicated over each spectra. The comparison of recovered structures from 14.0 and 16.5 GPa is given at the bottom of the figure.
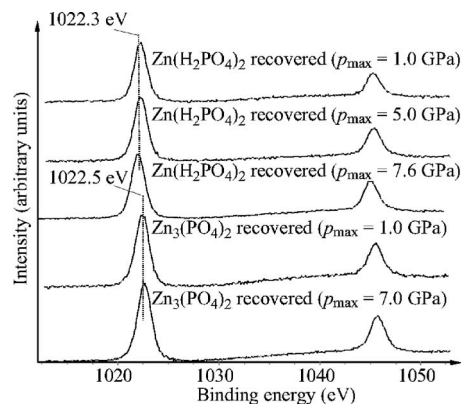

FIG. 10. X-ray photoelectron spectroscopy (XPS) measured on decompressed samples in order to probe the change of local arrangements on Zn. Neither zinc phosphate show any pressure-induced shift of binding energy (BE) of the zinc $2p$ electrons. XPS spectra on phosphorus and oxygen do not exhibit any pressure-induced shift of the BE (not shown).
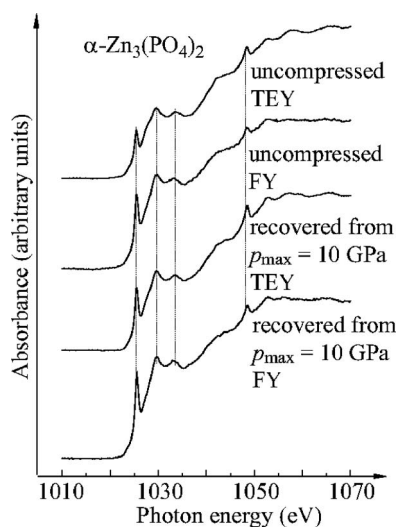
FIG. 11. X-ray absorption near edge structure (XANES) zinc L-edge spectra measured on decompressed samples probing the change of local arrangements on Zn. Neither zinc phosphate show any pressure-induced change of L-edge electron structure. XANES spectra on phosphorus do not show any pressure-induced change (not shown).
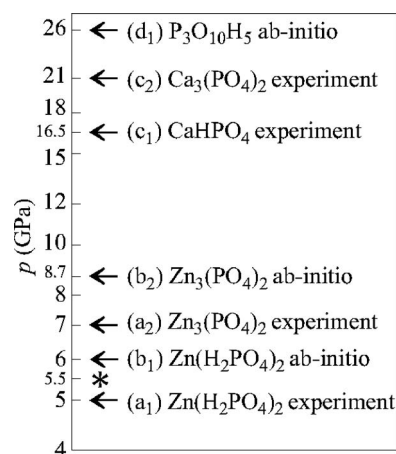

FIG. 12. Overview over various threshold pressures. Arrows indicate pressures where irreversible loss of long-range crystallinity takes place experimentally upon compression or where a coordination change is found in an *ab initio* study upon compression. The star indicates the pressure where *ab initio* calculations predict that compressed α-zinc phosphate reverts back to its low-pressure polymorph structure. Data points labeled (b1) and (d1) are taken from Refs. 8 and 28, respectively.

lowed by decompression to ambient pressures. No pressure-induced changes are observed; this clearly demonstrates the lack of any significant irreversible changes in the environment of the Zn^{2+} ion. Thus, spectroscopies sensitive to chemical bonding do not suggest any changes in the local order. This result was to be expected from the first-principles calculations on α-zinc phosphate presented in Fig. 2(c).

VII. CONCLUSIONS

In this paper, we investigated how crystalline zinc and calcium phosphates respond to external pressures. While the study was originally motivated by the desire to test the pressure-induced cross-linking theory for the formation and functionality of zinc phosphate containing antiwear films,[8] the lack of knowledge of the decomposition products of ZDDP involved in the film formation and the difficulty in synthesizing the decomposition model compounds used in the simulations create uncertainty as to whether the molecules we studied in both simulations and experiment are appropriate. Despite these reservations, the study of zinc phosphates with tetracoordinated zinc allows one to investigate some open questions related to the role that zinc phosphates' response to pressure may have in a tribological context because the coordination of zinc with oxygen in commercially available zinc phosphates strongly resembles that of the molecules found in the simulations after decompression. In addition, owing to the relevance of zinc phosphates in various fields, it is interesting to study the response of zinc phosphates to pressure in its own right.

The main results of our findings are summarized in Fig. 12, where we show the amorphization threshold pressures for various compounds. Most importantly, zinc phosphates "yield" at distinctly lower pressures than calcium or pure phosphates, and hydrogenated compounds yield earlier than nonhydrogenated materials.

The low pressure, at which the α-orthophosphate of zinc amorphizes, can be explained with its ability to change coordination. An orbital analysis reveals that zinc can grasp on to additional oxygen atoms by hybridizing a d orbital with a p orbital of a bridging oxygen into a σ bond. A similar hybridization may be responsible for a similarly low amorphization threshold of approximately 4.2 GPa in a pyrophosphate of cobalt.[36]

The direct comparison of first-principles calculations and experiments is satisfactory. The higher threshold pressures found in the simulations can be rationalized as a rate effect. Compression takes place at a rate of 10 GPa/ps in the simulations versus (order of magnitude) 0.1 GPa/s experimentally (plus the time required to acquire spectra). Thus, simulations probe the (mechanical/chemical) instability points, while thermal activation assists the transformations in the diamond anvil cell.

We would also like to point out that hydrogen-terminated pure phosphates yield at even higher pressures than hydrogen-free calcium phosphates. In the case of pure phosphates, valency changes on some of the phosphorus atoms from four to five upon compression. This makes us conclude that the phosphate unit itself is stable up to pressures of 26 GPa and that the disordering in the calcium phosphates must be due to changes associated with the cation. We abstained from simulating calcium phosphates directly due to the difficulty to produce good pseudopotentials for calcium.

It may be, though we clearly want to mark our closing paragraph as speculative, that the relatively low pressures at which zinc phosphates lose long-range order may benefit their functionality as antiwear agents for the following reason: the disordering reduces dislocation-driven plastic deformation and, thus, hardens the material. Supporting experimental evidence for this speculation may come from the following observation: Surfaces that are highly amorphized or disordered after "running-in," wear off at smaller rates than those with large crystalline domains.[37–40] Further ex-

perimental and theoretical examinations are certainly required to assess whether pressure-induced loss of crystallinity in zinc phosphate films really benefits their antiwear functionality.

ACKNOWLEDGMENTS

[1] V. F. Buchwald, *Phosphate Minerals* (Springer-Verlag, Berlin, 1984).

[2] X. Xie, M. Minitti, M. Chen, H. Mao, D. Wang, J. Shu, and Y. Fei, Geochim. Cosmochim. Acta **66**, 2439 (2002).

[3] U. Bismayer and W. G. Marshall, Acta Crystallogr., Sect. B: Struct. Sci. **60**, 1 (2004).

[4] R. J. Angel, U. Bismayer, and W. G. Marshall, J. Phys.: Condens. Matter **13**, 5353 (2001).

[5] L. Herschke, J. Rottstegge, I. Lieberwirth, and G. Wegner, J. Mater. Sci.: Mater. Med. **17**, 81 (2006).

[6] M. A. Nicholls, T. Do, P. R. Norton, M. Kasrai, and G. M. Bancroft, Tribol. Int. **38**, 15 (2005).

[7] M. A. Nicholls, G. M. Bancroft, P. R. Norton, M. Kasrai, G. D. Stasio, B. H. Frazer, and L. M. Wiesec, Tribol. Lett. **17**, 245 (2004).

[8] N. J. Mosey, M. H. Müser, and T. K. Woo, Science **207**, 1612 (2005).

[9] N. J. Mosey, T. K. Woo, M. Kasrai, P. R. Norton, G. M. Bancroft, and M. H. Müser, Tribol. Lett. **24**, 105 (2006).

[10] J. Tse, Y. Song, and Z. Liu, Tribol. Lett. **28**, 45 (2007).

[11] Z. Yin, M. Kasrai, M. Fuller, G. M. Bancroft, K. Fyfe, and K. H. Tan, Wear **202**, 172 (1997).

[12] M. Gauvin, F. Dassenoy, C. Minfray, J. M. Martin, G. Montagnac, and B. Reynard, J. Appl. Phys. **101**, 063505 (2007).

[13] M. Parrinello and A. Rahman, Phys. Rev. Lett. **45**, 1196 (1980).

[14] R. Car and M. Parrinello, Phys. Rev. Lett. **55**, 2471 (1985).

[15] J. Hütter, A. Alavi, T. Deutsch, M. Bernasconi, S. Gödecker, D. Marx, M. Tuckerman, and M. Parrinello, CPMD, version 3.5, IBM Zürich Research Laboratory and MPI für Festkörperforschung, 1995.

[16] W. Kohn and L. Sham, Phys. Rev. **140**, A1133 (1965).

[17] J. P. Perdew, K. Burke, and M. Ernzerhof, Phys. Rev. Lett. **77**, 3865 (1996).

[18] N. Troullier and J. L. Martins, Phys. Rev. B **43**, 1993 (1991).

[19] R. L. Frost, Spectrochim. Acta, Part A **60**, 1439 (2004).

[20] C. Ebner, U. Onthong, and M. Probst, J. Mol. Liq. **118**, 15 (2005).

[21] H. K. Mao, P. M. Bell, J. W. Shaner, and D. J. Steinberg, J. Appl. Phys. **46**, 543 (1978).

[22] B. M. Nirsha, T. V. Khomutova, A. A. Fakeev, B. V. Zhadanov, V. M. Agre, N. P. Kozlova, and V. A. Olikova, Russ. J. Inorg. Chem. **27**, 630 (1982).

[23] B. X. Yang, F. H. Middleton, B. G. Olsson, G. M. Bancroft, J. M. Chen, T. K. Sham, K. Tan, and D. J. Wallace, Rev. Sci. Instrum. **63**, 1355 (1992).

[24] M. Kasrai, Z. Yin, G. Bancroft, and K. Tan, J. Vac. Sci. Technol. A **11**, 2694 (1993).

[25] M. A. Nicholls, T. Do, P. R. Norton, G. M. Bancroft, M. Kasrai, T. W. Capehart, Y. T. Cheng, and T. Perry, Tribol. Lett. **15**, 241 (2003).

[26] G. Pereira, A. Lachenwitzer, M. Nicholls, M. Kasrai, P. Norton, and G. D. Stasio, Tribol. Lett. **18**, 411 (2005).

[27] N. J. Mosey, T. K. Woo, and M. H. Müser, Phys. Rev. B **72**, 054124 (2005).

[28] R. K. Brow, D. R. Tallant, S. T. Myers, and C. C. Phifer, J. Non-Cryst. Solids **191**, 45 (1995).

[29] J. Amami, M. Ferid, and M. Trabelsi–Ayedi, Mater. Res. Bull. **40**, 2144 (2005).

[30] M. E. Masloumi, I. Imaz, J.-P. Chaminade, J.-J. Videau, M. Couzi, M. Mesnaoui, and M. Maazaz, J. Solid State Chem. **178**, 3581 (2005).

[31] M. Najman, M. Kasrai, G. M. Bancroft, and R. Davidson, Tribol. Int. **39**, 342 (2006).

[32] M. Kasrai, M. Fuller, G. M. Bancroft, E. S. Yamaguchi, and P. R. Ryason, Tribol. Trans. **49**, 3276 (2003).

[33] M. Kasrai, M. Suominen–Fuller, G. M. Bancroft, E. S. Yamaguchi, and P. R. Ryason, Tribol. Trans. **46**, 543 (2003).

[34] P. Kapsa, J. M. Martin, C. Blanc, and J. M. Georges, Trans. ASME **103**, 486 (1981).

[35] G. Pereira, A. Lachenwitzer, D. Munoz–Paniagua, M. Kasrai, P. R. Norton, T. W. Capehart, T. A. Perry, and Y. T. Cheng, Tribology Materials, Surfaces and Interfaces **1**, 4 (2007).

[36] M. Baril, H. Assaaoudi, and I. S. Butler, J. Mol. Struct. **751**, 168 (2005).

[37] S. K. Ganapathi and D. A. Rigney, Scr. Metall. Mater. **24**, 1675 (1990).

[38] D. Shakhvorostov, K. Pöhlmann, and M. Scherge, Wear **260**, 433 (2006).

[39] M. Belin, J. M. Martin, and J. L. Mansot, Tribol. Trans. **32**, 410 (1989).

[40] S. Fukumoto, H. Tsubakino, K. Okita, M. Aritoshi, and T. Tomita, Scr. Mater. **42**, 807 (2000).